NASA CR-54141
AI-64-153

N7372053

FINAL REPORT
THERMAL PROPERTIES
OF
TUNGSTEN-URANIUM DIOXIDE MIXTURES
(U)

By
R.E. TAYLOR

Prepared for
NATIONAL AERONAUTICS AND SPACE ADMINISTRATION
SEPTEMBER 1, 1964
CONTRACT NAS 3-4280

Technical Management
NASA Lewis Research Center
Cleveland, Ohio
Materials and Structures Division
R.J. BUZZARD

ATOMICS INTERNATIONAL
A DIVISION OF NORTH AMERICAN AVIATION, INC.
P.O. BOX 309 CANOGA PARK, CALIFORNIA

REPRODUCED BY: NTIS
U.S. Department of Commerce
National Technical Information Service
Springfield, Virginia 22161

ABSTRACT

The thermal expansion, density, thermal diffusivity, and specific heat of various tungsten-uranium dioxide composites were measured from room temperature to very high temperatures. Because of the sample geometry, it was necessary to account for the finite pulse time effects in the thermal diffusivity measurements. The mathematical expression for a square wave energy input was derived and experimentally verified. Thermal conductivity values were calculated from the density, specific heat, and diffusivity results.

CONTENTS

FIGURES

THERMAL PROPERTIES OF TUNGSTEN-URANIUM DIOXIDE MIXTURES

by

R. E. Taylor
Atomics International
Div. North American Aviation, Inc.

SUMMARY

The objective of this program was to determine the thermal expansion and thermal conductivity, from room temperature to 5000°F, of four composites (viz: 10, 20, 30, and 40 vol %) of uranium dioxide in a tungsten matrix.

The thermal expansions of the four composites were measured over this temperature interval, and equations for the results are given. The agreement between measured and calculated values is generally within 5%; but in a few cases, is as high as 8%. The expansions of these mixtures are, as expected, very close to that of pure tungsten.

The thermal conductivity was not measured directly. Instead, the diffusivities of the various mixtures were measured, and the thermal conductivities were calculated as the product of the specific heat, density, and diffusivity. The density and diffusivity were not corrected for thermal expansion. The expansion increases the diffusivity by the square of the increase in length of the sample, and decreases the density by the cube of this quantity. Consequently, the net effect is a 2% error in the thermal conductivity values at high temperatures. Since this is well within the ±9% uncertainty in the conductivity, it was considered unnecessary to correct the density and diffusivity values.

Conductivity values were also calculated using the Bruggeman variable-dispersion equation. These results are higher than the experimental values obtained from this study, partly because of anisotropic effects. In addition, the thermal conductivity of tungsten is not known accurately, and this may be the cause of some of the discrepancy.

The electrical resistivity of the 80 W - 20 UO_2 mixture was measured, and the results were used to calculate the contribution of free electrons to the total conductivity. It was found that the major portion of the heat transport is due to electrons.

I. INTRODUCTION

Space mission analyses indicate that the thrust requirements of some space exploration vehicles can be met through the use of nuclear propulsion systems. Advanced concepts of nuclear rockets require high operating temperatures for higher thrust and lower engine weights. A thermal nuclear rocket concept is presently being studied at the Lewis Research Center of NASA.[1] This concept is based on the use of tungsten-uranium dioxide (W-UO_2) composites for the fuel element materials. These composites are currently being fabricated in the form of plates which are useful in initial studies to determine the behavior of this combination of materials at elevated temperatures.

To aid preliminary design analysis of this reactor concept, a knowledge of the properties of W-UO_2 composites is desirable. For this purpose, high-temperature mechanical properties of various W-UO_2 composites are being determined at the Lewis Research Center.[2] Certain physical properties of various W-UO_2 composites have been studied at Atomics International, under NASA contract NAS3-4280. The specific objective of this study was to determine the thermal expansion and thermal conductivity values from room temperature to 5000°F for four compositions (viz., 10, 20, 30, and 40 vol %)* of uranium dioxide dispersed in a tungsten matrix. Since these values are highly dependent on the size and nature of the dispersed particles and on the fabrication history of the composites, the values determined in this program are to be considered only as indicative of the properties of the materials to be used in the actual fuel elements.

The present report constitutes the final technical summary of the experimental work performed in this physical property evaluation program. In this study, the thermal expansivities of four W-UO_2 composites were determined directly, by measuring the relative linear displacements of plate-type specimens as a function of temperature. Although thermal conductivities can also be measured directly, the sample configuration was not amenable to this type of measurement. Therefore, to simplify the thermal conductivity determinations, this property

*In this report, percentages are expressed as volume percent (vol%), and tungsten is listed first.

was obtained by measuring the thermal diffusivity (α), and calculating the thermal conductivity (k) from the relation:

$$k = \alpha c_p d \quad , \qquad \ldots(1)$$

where c_p is the specific heat and d is the density. Since this method is as reliable as measuring the thermal conductivity directly, the former method was chosen for this program. This technique required measurement of density, thermal diffusivity, and specific heat. The results of these measurements are reported herein.

a. 90 W - 10 UO_2
(Photo Supplied by NASA)

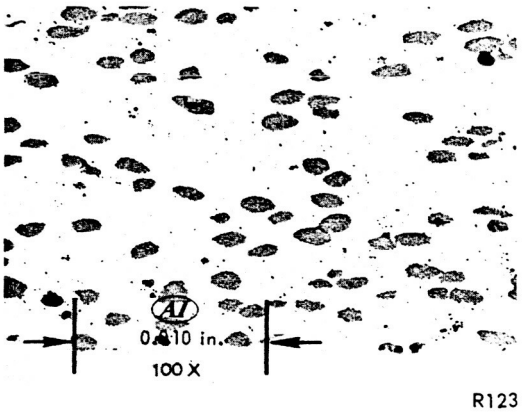

b. 80 W - 20 UO_2

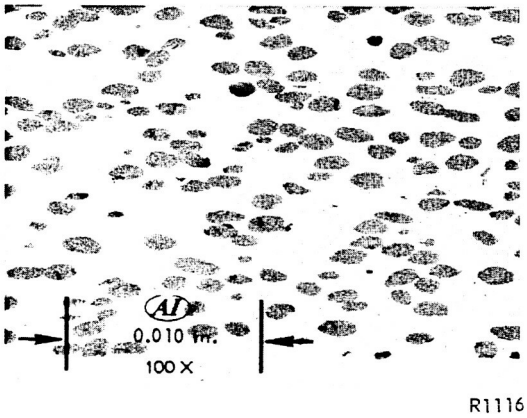

c. 70 W - 30 UO_2

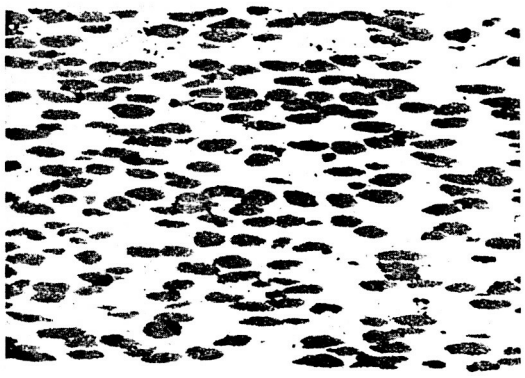

d. 60 W - 40 UO_2
(Photo Supplied by NASA)

Figure 1. Photomicrographs of W-UO_2 Mixtures

II. MATERIALS

The test materials used in this study were fabricated in the form of plates, about 0.030 in. thick. Powder metallurgy techniques are used to produce sintered compacts of about 60% of theoretical density. Batch sintering these compacts in hydrogen at 3150°F results in a densification to about 92% of theoretical density. The compacts are clad with tungsten, to retain the fuel, and hot rolled to produce a very dense structure.[3] Photomicrographs of samples of W - UO_2 mixtures are shown in Figure 1. The UO_2 is visible as randomly distributed spheroids.

The densities of the samples used in this study were determined by the standard water displacement method. These results are summarized in Appendix I, and are compared to the theoretical values in Figure 2. The densities of the 70-30 and 60-40 mixtures are greater than the theoretical density

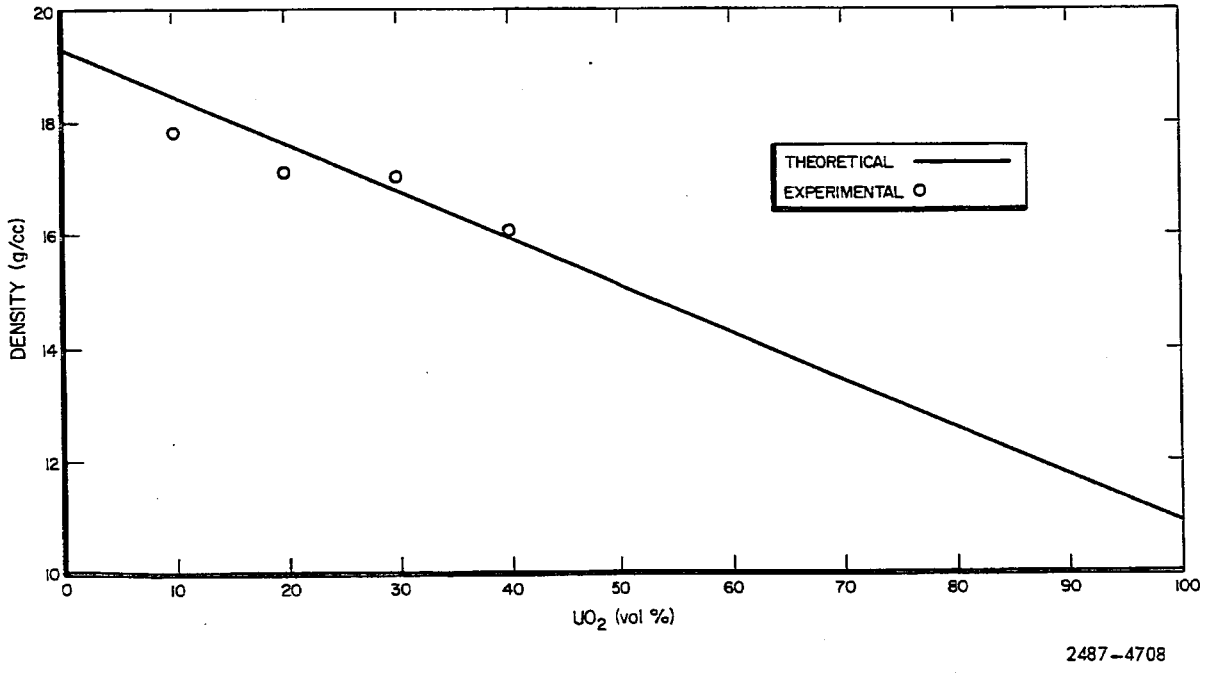

Figure 2. Density of W-UO_2 Mixtures

for W-UO_2 compacts due to the tungsten cladding on the surfaces of the samples. Because of the small sample size used for the 70-30 mixture (<0.2 g, Appendix I), the density obtained for this mixture may not be representative of the bulk material of this composition. Since the density values obtained in this study are close to the theoretical density of the material, the theoretical values were used for conductivity calculations.

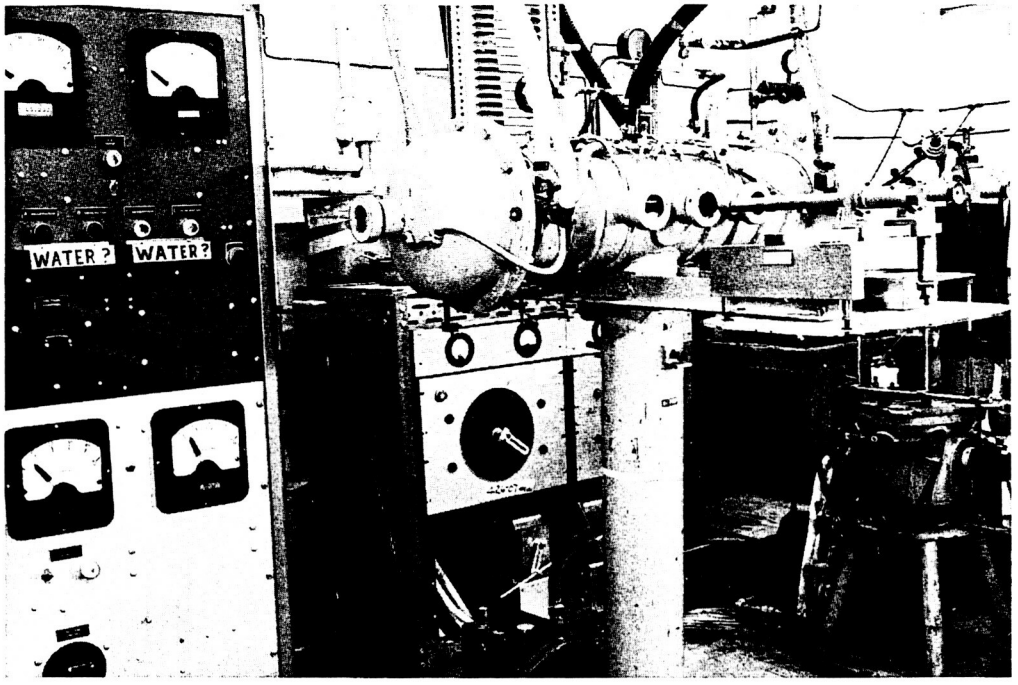

7513-1884

a. Photograph

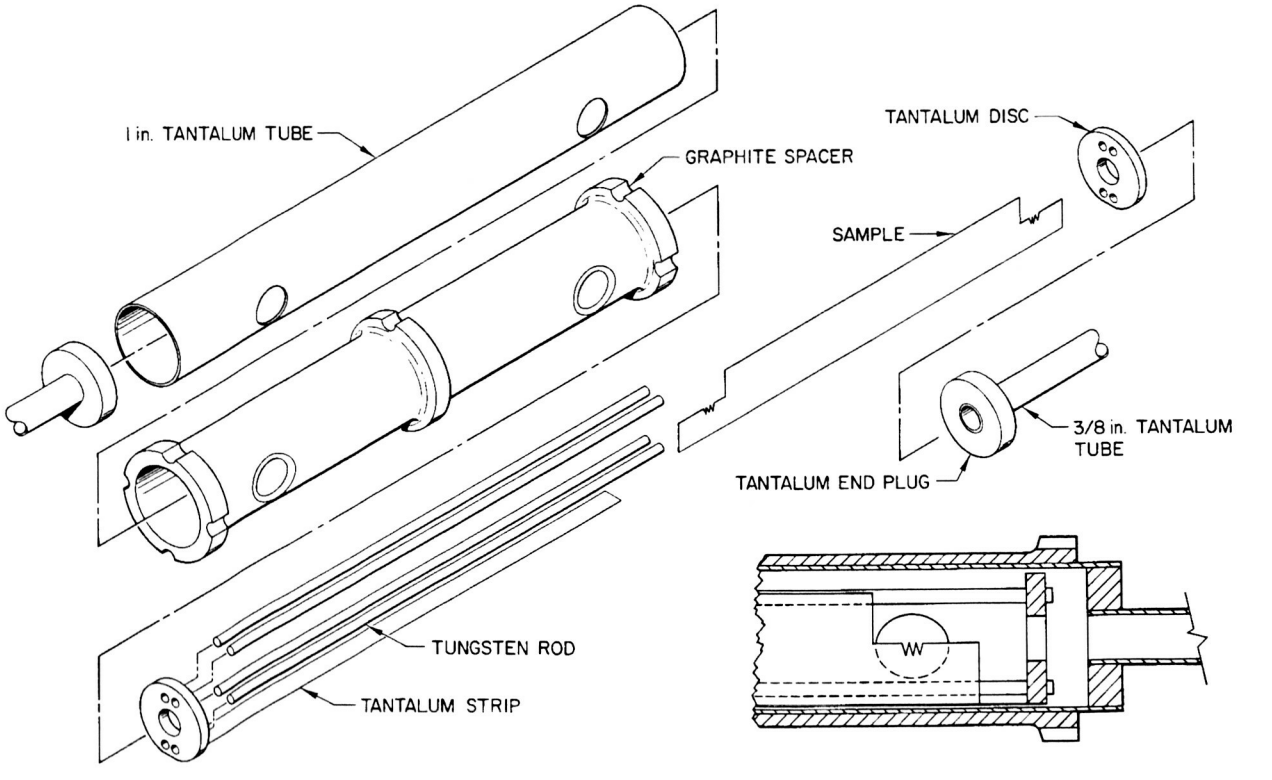

2487-4725

b. Specimen Holder

Figure 3. Thermal Expansion Furnace
(Figures Unclassified)

III. THERMAL EXPANSION

A. APPARATUS AND EXPERIMENTAL PROCEDURES

The test equipment for measuring linear thermal expansions to very high temperatures is described in detail in the literature.[4] Measurements are made by observing the relative displacements of fiducial marks on the opposite ends of 5-in. long specimens as they are heated in a graphite tube furnace. Displacements are measured with two telescopes fitted with filar eyepieces, capable of accurately and reproducibly measuring to ±0.00005 in. Samples are usually allowed to expand freely on a tungsten holder, within a tantalum tube which protects them from contamination. The furnace atmosphere is controllable from vacuum (1 mm Hg) to 200 psi. Often, dried argon at 50 psi is used. Generally, about 2 hr are required to reach a new set temperature and stabilize the furnace. The thermal gradient across the sample varied with temperature, being about 60°F at 1000°F and 20°F at 2000°F.

This apparatus, which is shown in Figure 3, has been used to measure the expansions of molybdenum, tantalum, and graphite to 6500°F.[5] Recently, data on the carbides of silicon, boron, and titanium, as well as the oxides of aluminum, magnesium, and beryllium, were obtained.[6,7]

B. RESULTS

The results for the 90-10, 80-20, and 70-30 mixtures are presented in Figure 4. The coefficient of expansion of the mixtures increases with increasing UO_2 content. However, the expansion of all of these mixtures is much closer to that of pure tungsten than it is to an averaged expansion of tungsten and UO_2. In fact, the expansion of the 90-10 mixture is very close to the expansion of pure tungsten.[8] For example, at 2190°F, the expansion of W is 0.60% and that of the 90-10 mixture is 0.605%, while the expansion of UO_2 is 1.27% at this temperature.[9] An average expansion of the 80-20 mixture is 0.74% at 2190°F, while the observed expansion is only 0.64%. The expansion of the 70-30 composition is very close to that of the 80-20 composition.

The least-square equations for the expansion of the 90-10, 80-20, and 70-30 compositions, for $60°F < t\ (°F) < 5000°F$, are:

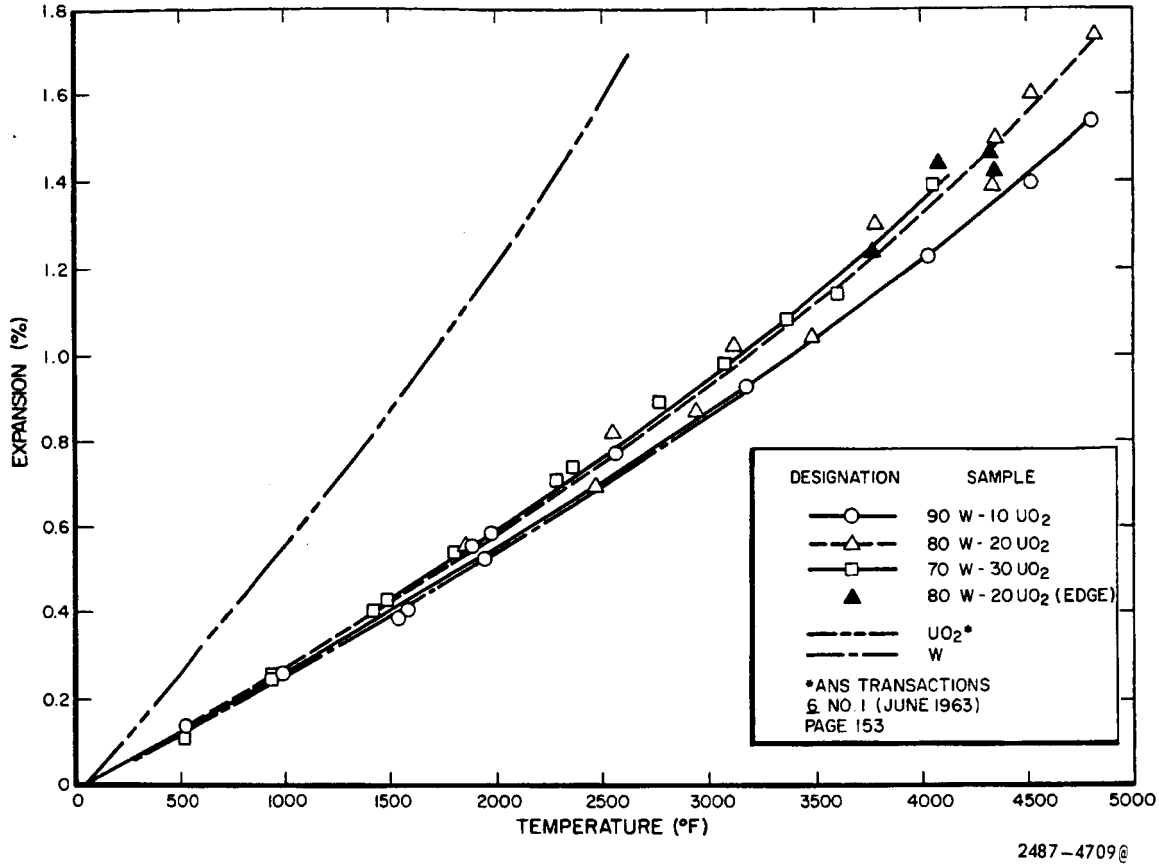

Figure 4. Thermal Expansion of 90 W - 10 UO_2, 80 W - 20 UO_2, and 70 W - 30 UO_2 Mixtures

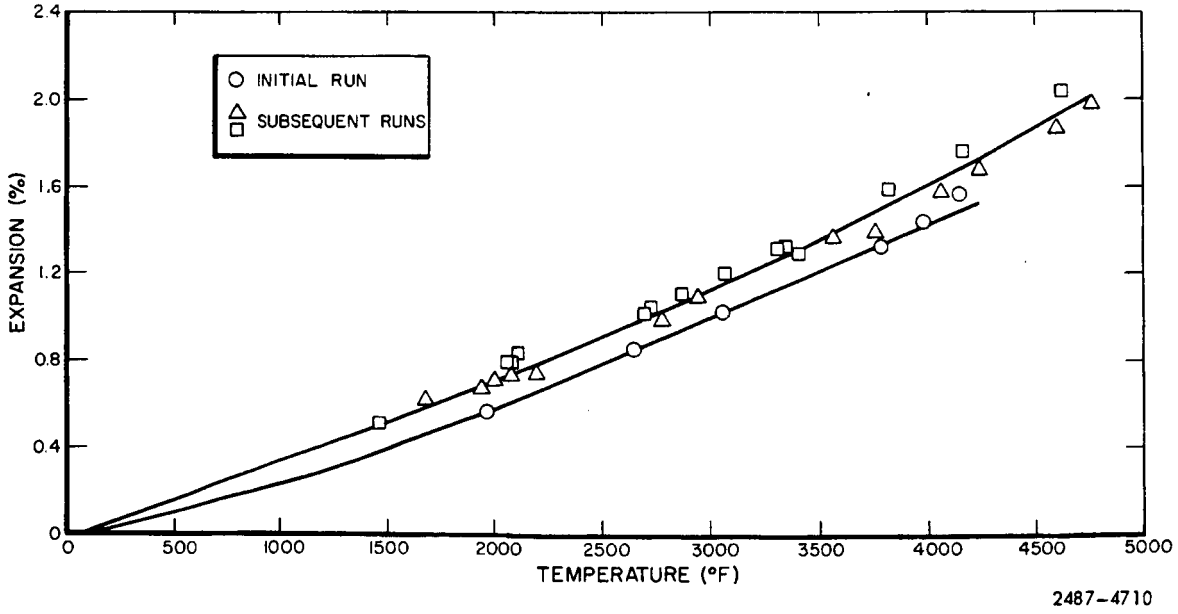

Figure 5. Thermal Expansion of 60 W - 40 UO_2 Mixtures

$$90\text{-}10\text{: \% expansion} = -1.748 \times 10^{-2} + 2.8997 \times 10^{-4} t - 3.5932 \times 10^{-9} t^2 + 2.1028 \times 10^{-12} t^3 \quad \ldots(2)$$

$$80\text{-}20\text{: \% expansion} = -2.321 \times 10^{-2} + 3.9013 \times 10^{-4} t - 6.0273 \times 10^{-8} t^2 + 1.1362 \times 10^{-11} t^3 \quad \ldots(3)$$

$$70\text{-}30\text{: \% expansion} = -1.7124 \times 10^{-2} + 2.8387 \times 10^{-4} t + 1.08175 \times 10^{-8} t^2 + 7.4091 \times 10^{-13} t^3 \quad \ldots(4)$$

These equations are plotted with the experimental data in Figure 4.

By differentiating these equations with respect to t, and accounting for the factor of 100 which changes percent expansion to the decimal, one obtains the equations which express the coefficient of expansion as a function of temperature for each of these compositions:

$$90\text{-}10\text{: coeff. of expansion} = 2.8997 \times 10^{-6} - 7.1864 \times 10^{-11} t + 6.3084 \times 10^{-14} t^2 \quad \ldots(5)$$

$$80\text{-}20\text{: coeff. of expansion} = 3.9013 \times 10^{-6} - 1.20546 \times 10^{-9} t + 3.4086 \times 10^{-13} t^2 \quad \ldots(6)$$

$$70\text{-}30\text{: coeff. of expansion} = 2.8387 \times 10^{-6} + 2.16350 \times 10^{-10} t + 2.22273 \times 10^{-14} t^2 \quad \ldots(7)$$

For example, the coefficient of expansion of the 90-10 mixture at 2000°F is 3.01×10^{-6}/°F.

The initial expansion of one of the samples of the 60-40 mixture, (circles on Figure 5) was very close to that of the 80-20 and 70-30 compositions. However, the thermal expansion measured during subsequent runs on the same specimen

(triangles, Figure 5) and for all runs on a second sample (squares, Figure 5) were appreciably above the initial values. The reason for this behavior is not understood, but may be due to stress-relief during the initial heating to 4200° F. The equation for the expansion, measured during all but the one initial run, is

$$60\text{-}40\text{: \% expansion} = -2.3323 \times 10^{-2} + 3.8906 \times 10^{-4} t - 1.4755 \times 10^{-8} t^2 + 4.8042 \times 10^{-12} t^3 \quad \ldots(8)$$

The expansion of the 80-20 material was measured in the width direction at high temperatures. Due to the sample dimensions, it was not possible to measure the expansion below 3700° F with sufficient accuracy. However, the data above that temperature show that the expansion is isotropic. These data points are included on Figure 4.

IV. SPECIFIC HEAT

A. CALCULATED VALUES

Specific heat values of the various composites were obtained by suitable averaging of the specific heats of the two components (Knoop's rule). Fortunately, the specific heats of tungsten and UO_2 are known to within a few percent.[10,11] Consequently, the calculated specific heats should be accurate to within ±4%. The results are plotted in Figure 6.

B. ENTHALPY

The most common technique for determining the specific heat is to measure the increase in enthalpy as a function of temperature, by means of a drop calorimeter. The specific heat, which is the slope of the enthalpy curve, may then be determined graphically or by differentiating the equation which expresses the enthalpy data. In order to check the validity of the specific heat calculations, the reverse procedure was followed (i.e., the equation which expresses the specific heat of the 80-20 mixture was obtained by a computer, and was integrated to obtain enthalpy values which were checked against experimental enthalpy values). The results are plotted in Figure 7. The enthalpy was experimentally measured by Thermatest Laboratories. Three of the enthalpy points had large errors associated with them, because the enthalpy of the graphite crucible used to hold the sample constituted an appreciable portion of the total measured enthalpy. The other points, which were obtained using a copper crucible, were subject to much less error, because of the smaller enthalpy of the copper crucible. When the normal measuring errors, which are estimated at ±5%, are added to the uncertainties caused by the enthalpy of the crucible, the enthalpy values overlap the calculated values above 800° F. Consequently, the calculated specific heat results were used in the subsequent thermal conductivity calculations.

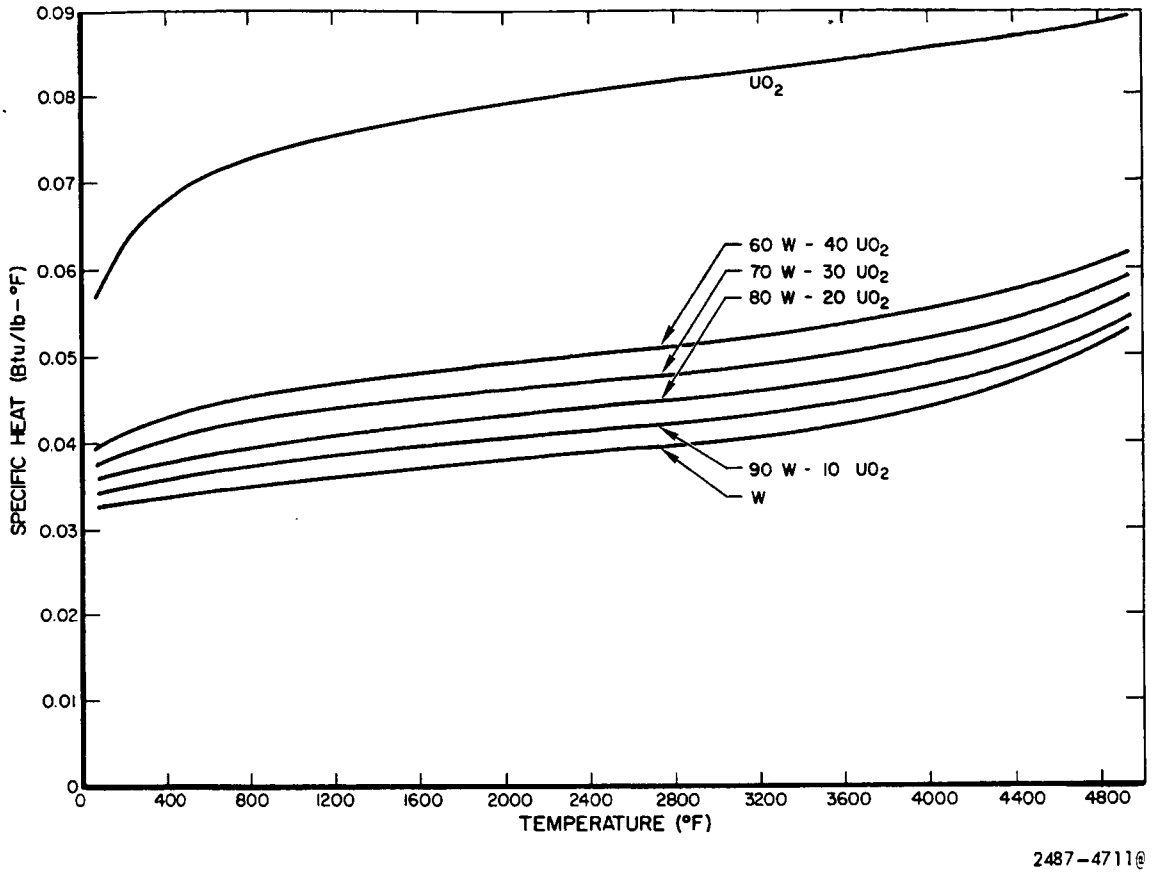

Figure 6. Specific Heat of W-UO_2 Mixtures

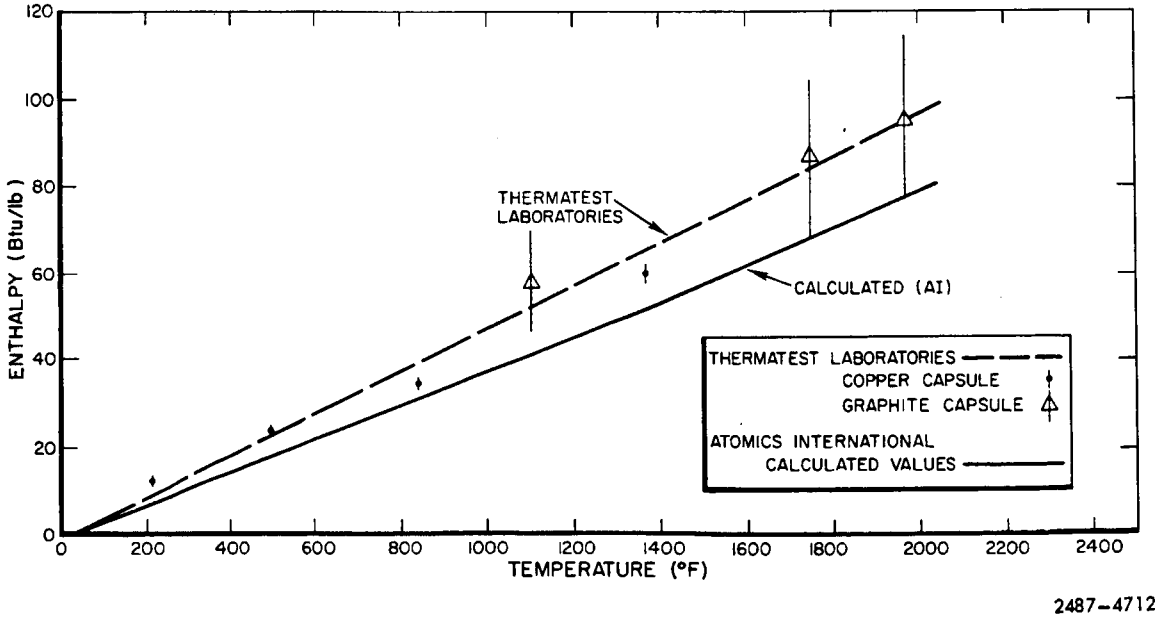

Figure 7. Enthalpy of 80 W - 20 UO_2 Mixtures

V. THERMAL DIFFUSIVITY

A. APPARATUS

The flash diffusivity method, which was originally described by Parker et al.,[12] was used for the thermal diffusivity measurements. In this method, a pulse of energy is radiated to the front face of a disk-shaped sample, and the resulting temperature history of the rear face is used to determine a diffusivity value. The ambient temperature of the sample is controlled by a tantalum tube heater, and the pulse of energy raises the average sample temperature only a few degrees.

In the original description by Parker et al.,[12] a xenon flash lamp was used as the energy source However, the flash lamp is limited by the fact that the emitting area is so large that optically focusing the energy on a small specimen is not very practical. Therefore, one must keep the flash lamp near the sample, which is not convenient at high sample temperatures. On the other hand, a laser efficiently concentrates the flash lamp energy into a coherent light beam, well suited for irradiating small samples which are enclosed within vacuum furnaces. Consequently, our laboratory uses a laser beam energy source for the flash diffusivity apparatus.

The rear face sample temperature is measured with thermocouples up to 3100° F, and with a photoelectric detector at higher temperatures. Both PbS and photomultiplier tubes have been used as detectors. Since the recording pyrometer has been described in a recent article,[13] it will not be discussed here.

The apparatus is shown in Figure 8. A vacuum chamber (not shown) fits over the tantulum tube heater and shield. The mounted sample and radiation shields are shown near the heater. During a measurement, the sample and holder are placed inside the tube heater. The laser is shown in the lower left hand corner of the photograph, and the recording pyrometer is shown lined up with the laser and the tube furnace. The vacuum system is located beneath the table.

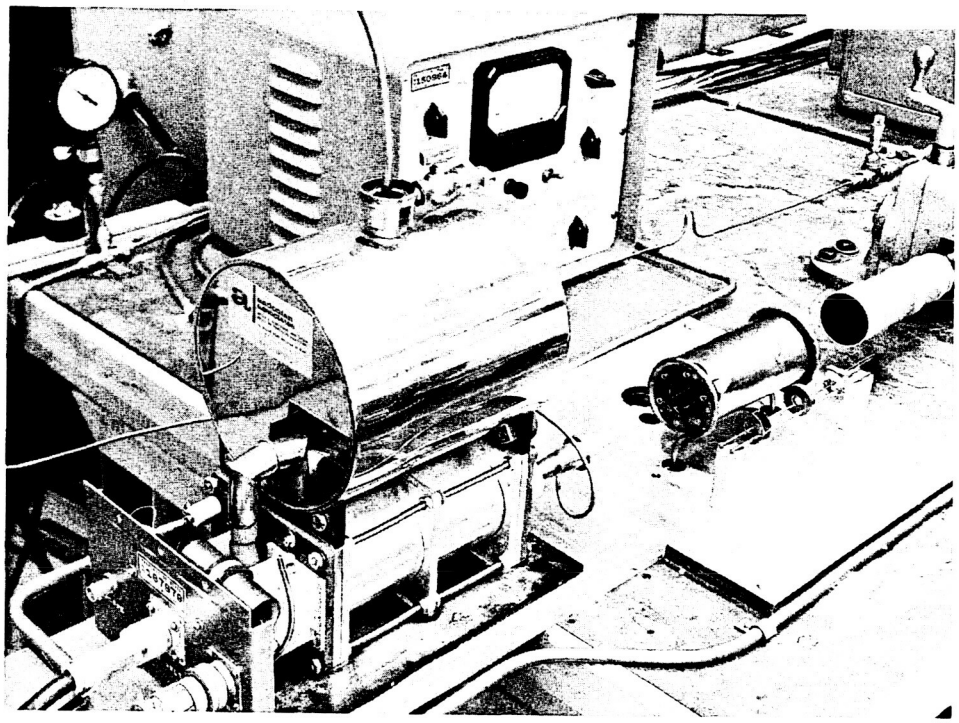

7516-1846

a. Photograph

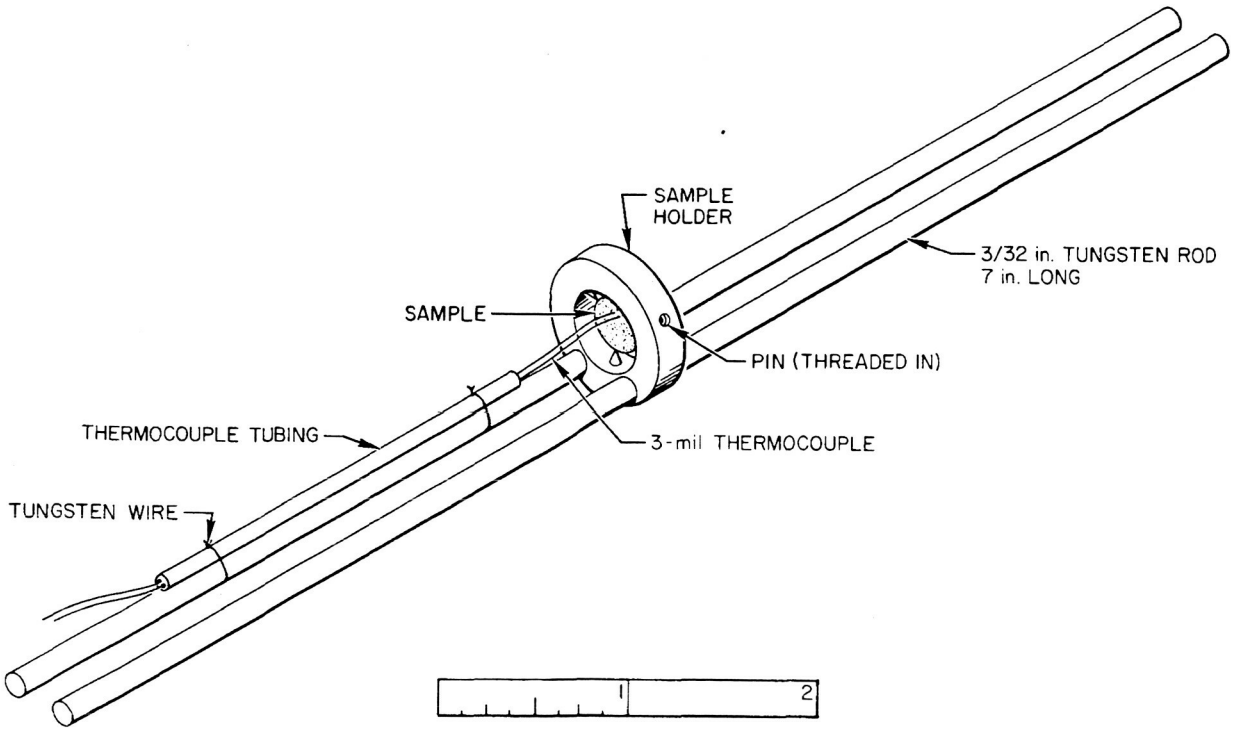

2487-4726

b. Specimen Holder

Figure 8. Thermal Diffusivity Apparatus
(Figures Unclassified)

B. FINITE PULSE TIME EFFECT

From the transient response of the rear face temperature, the simple relation

$$\alpha = 1.37\, a^2/\pi^2 t_{1/2} \qquad \ldots(9)$$

was obtained by Parker et al., where $t_{1/2}$ is the time required for the backface to reach one-half of its maximum temperature rise, and a is the sample thickness. The derivation of Equation 9 assumes that the energy pulse is received within a time duration (τ), which is short compared to characteristic rise time (t_c) given by

$$t_c = a^2/\pi^2\alpha \qquad \ldots(10)$$

Normally, one chooses an appropriate thickness for a given material, such that $t_c > 50\,\tau$, and Equation 9 is then obeyed within 2%. However, in the present case, the sample thickness had to be held constant. Since the diffusivity of each mixture is a fundamental property of the material, the characteristic time was fixed for each sample at each temperature. Of course, the characteristic times varied with composition and temperature. However, the range of characteristic times for these materials was from 1 to 7 msec. Consequently, in order to apply Equation 9, τ should be from 0.02 to 0.14 msec. Since the normal duration of the laser burst is from 1.1 to 1.7 msec, this condition is not met. It is possible to shorten the laser pulse by means of "Q" spoilers. This in an expensive and inefficient operation. In fact, about 90% of the available energy is lost, making it difficult to produce a sample temperature rise sufficient for accurate measurements. In addition, extremely rapid response thermocouples and amplifiers are required for the measurements. Consequently, the mathematical expression which expresses the heat flow was modified to take into account the finite pulse time effect.

The general equation which expresses the heat flow in a thin wafer subjected to an energy pulse on one side was solved by J. Cape and G. Lehman of our laboratory.[14] This equation takes into account both the finite pulse time effect and radiation losses from the edges. Cape and Lehman solved the radiationless

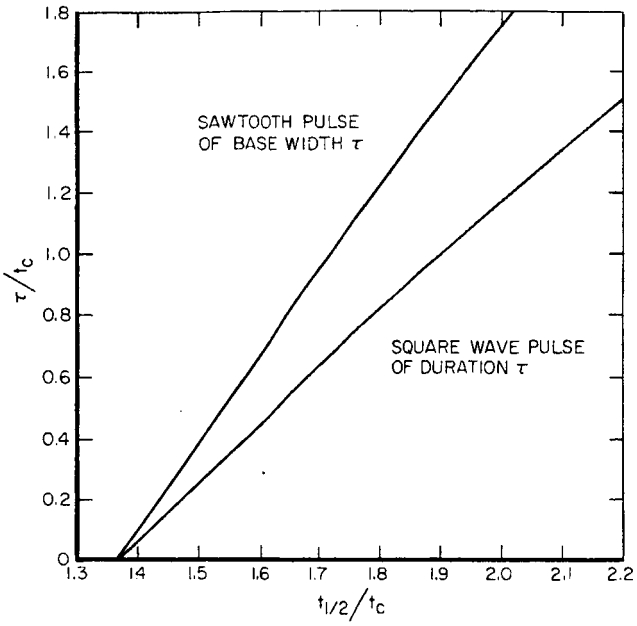

Figure 9. Finite Pulse Time Corrections (Figure Unclassified)

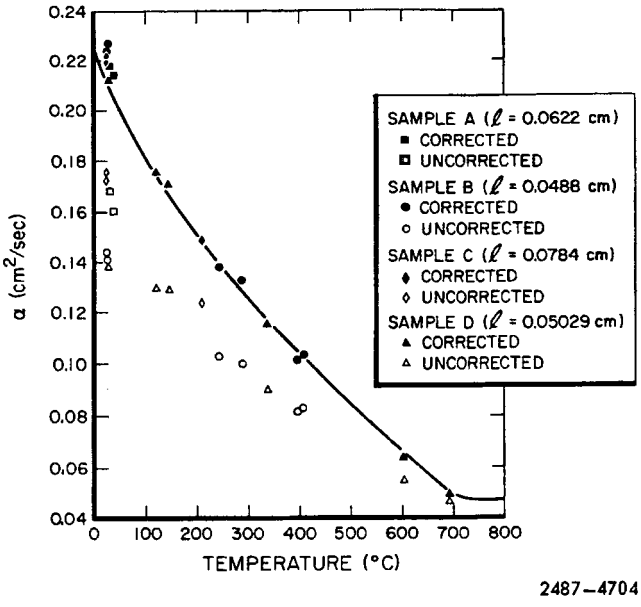

Figure 10. Thermal Diffusivity of Thin Samples of Armco Iron (Figure Unclassified)

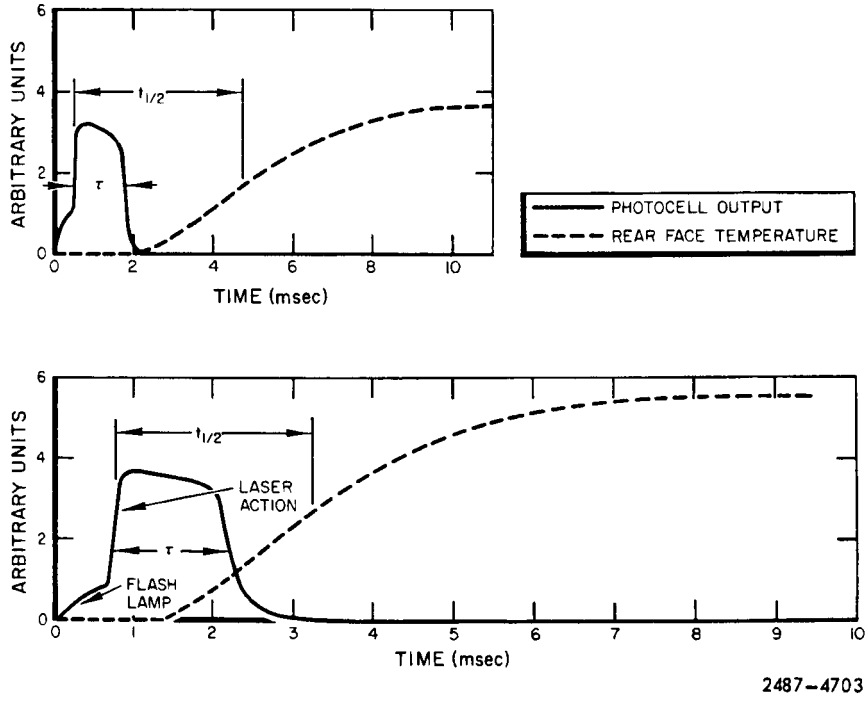

Figure 11. Response of Photocell and Rear Face Temperature (Figure Unclassified)

case for a finite sawtooth pulse. However, an examination of the laser pulse revealed that it closely approximated a square wave. Therefore, it was necessary to solve the general expression for a square wave energy input. This is done in Appendix III.

Because there are three variables (t_c, τ, and t) instead of two, it is not possible to plot t/t_c vs $\delta(a,r,t)/\delta(a,r,\infty)$ where $\delta(a,r,t)/\delta(a,r,\infty)$ is the ratio of the rear face temperature rise to the maximum rise, as Parker et al. did when they determined that, when this ratio equals 0.5:

$$t = t_{1/2} = 1.37\, t_c \qquad \ldots(11)$$

When one substitutes Equation 10 into Equation 11, one obtains Equation 9, which is the expression used to calculate diffusivities from the experimentally measured half-time when τ is small compared to t_c. In the present case, however, it is possible to plot τ/t_c vs $t_{1/2}/t_c$, to yield a curve which can be used to calculate t_c, and hence α, from the experimentally measured values of τ and $t_{1/2}$. In order to obtain such a curve, one must first plot values of $\delta(a,r,t)/\delta(a,r,\infty)$ for selected values of τ/t_c, by varying the values of t/t_c in Equation 22 (Appendix III). From these plots, the value of $t_{1/2}/t_c$ is determined for each of the selected values of τ/t_c.

The graphs of τ/t_c vs $t_{1/2}/t_c$ for a square wave and sawtooth energy pulse are shown in Figure 9. The curve for the square wave energy input shows, for example, that, when the pulse time is 0.8 of the characteristic time, the numerical factor is 1.785, instead of the 1.37 value used when pulse times are short compared to the characteristic time. For this particular case, then, an error of 30% is involved in neglecting the effect of the finite pulse time.

The validity of the described procedure was verified experimentally using Armco iron, which is the generally accepted thermal conductivity standard. Since the diffusivity of Armco iron decreases rapidly with increasing temperature, the characteristic time has a strong temperature dependency. Of course, the characteristic time can also be changed by varying the sample thickness. Consequently, it is possible to check the mathematics by either measuring the diffusivity of samples of different thickness or by measuring the diffusivity of the same sample at different temperatures. Both methods were used to obtain the results shown in Figure 10. The solid line represents the literature value,

the solid points represent the values obtained from the experimental values of τ and $t_{1/2}$, and the unfilled points represent the uncorrected data. These data represent values of τ/t_c ranging from 0.3 to 1.5. Some of the values at room temperature are in error; because the laser pulse is not a true square wave, but lies somewhere between a square wave and a sawtooth function. This is illustrated in Figure 11, which shows the photocell output from the time the flash lamp fires until the output returns to its base line, and also shows the rear face temperature response. For the first 1/2 msec following the initiation of the flash lamp discharge, the laser crystal acts as a "light pipe." Although this energy is apparent to the photocell, it is insignificant as far as heating the sample is concerned, and the pulse width and half-time are measured from the initiation of the laser action, as indicated in the figure. The experimental curves from two separate experiments are shown in Figure 11. The half-time measured from the lower curve can be expected to be influenced to a greater extent by the deviation of the laser pulse from a true square wave, since the rear face temperature is rising during the laser action. Consequently, the true correction for this curve lies between the correction curves for the square and sawtooth energy pulses shown in Figure 9. This causes the corrected data to be several percent high when the half-time is only 1.5 times the pulse width.

C. RESULTS

It was planned originally to use the photoelectric pyrometer for the high-temperature (i.e., > 2500°F) measurements, and thermocouples for the low-temperature measurements. However, the photoelectric pyrometer went into saturation for 10 msec following the laser pulse. While this does not interfere with obtaining results on samples of 0.1 in. thickness, where the rise time is usually several hundred milliseconds, it prevented the obtaining of data for the thin samples, since their rise time is less than 10 msec. Although this problem could be overcome by modifying the apparatus and obtaining a set of laser interference filters, cost and time elements prevented this being done within the scope of the present contract. Consequently, the measurements were limited to the use of thermocouples. However, tungsten-tungsten/26% rhenium thermocouples were substituted for the Chromel-Alumel thermocouples, in order to extend the practical range to 3800°F. The diffusivity data are so well-behaved that the results can be confidently extrapolated to at least 4500°F, and this was done for the purpose of estimating the thermal conductivity up to this temperature.

The results for two samples of the 90-10 mixture are shown in Figure 12. The diffusivity decreases smoothly from 0.471 cm^2/sec at 100°C (212°F) to 0.220 cm^2/sec at 2000°C (3632°F). The maximum scatter in the data from the smooth curve is 10%, and the usual scatter is within 5%.

The results for the 80-20 mixture are shown in Figure 13. Two different thicknesses (0.0281 and 0.0605 in.) were used in these experiments. Since the thickness enters into the equation as the square term, the use of these two thicknesses is equivalent to changing the experimental conditions by a factor of four. Consequently, the agreement between the results for the two thicknesses constitutes a verification of the experimental values. The diffusivity of the 80-20 mixture decreases from 0.313 cm^2/sec at 100°C to 0.197 cm^2/sec at 2000°C.

The diffusivity of the 80-20 mixture was also measured in the length direction, and it was found to be significantly greater than that measured in the width direction. This is shown in Figure 13. Because of the sample geometry, measurements made in the length direction do not require the finite pulse time correction discussed previously. However, due to heat loss from the sides of the specimen, the measurements are limited to low temperatures. Nevertheless, the measurements show that the thermal conductivity, unlike the thermal expansion, is anisotropic, with the thermal conductivity in the length direction being 20 ± 10% greater than the conductivity in the width direction.

The results for the thermal diffusivity of the 70-30 mixture are given in Figure 14, and the results for the 60-40 mixture are given in Figure 15. The reproducibility of these data is better than that obtained on the 90-10 and 80-20 mixtures, because of the lower diffusivities and consequently longer characteristic times.

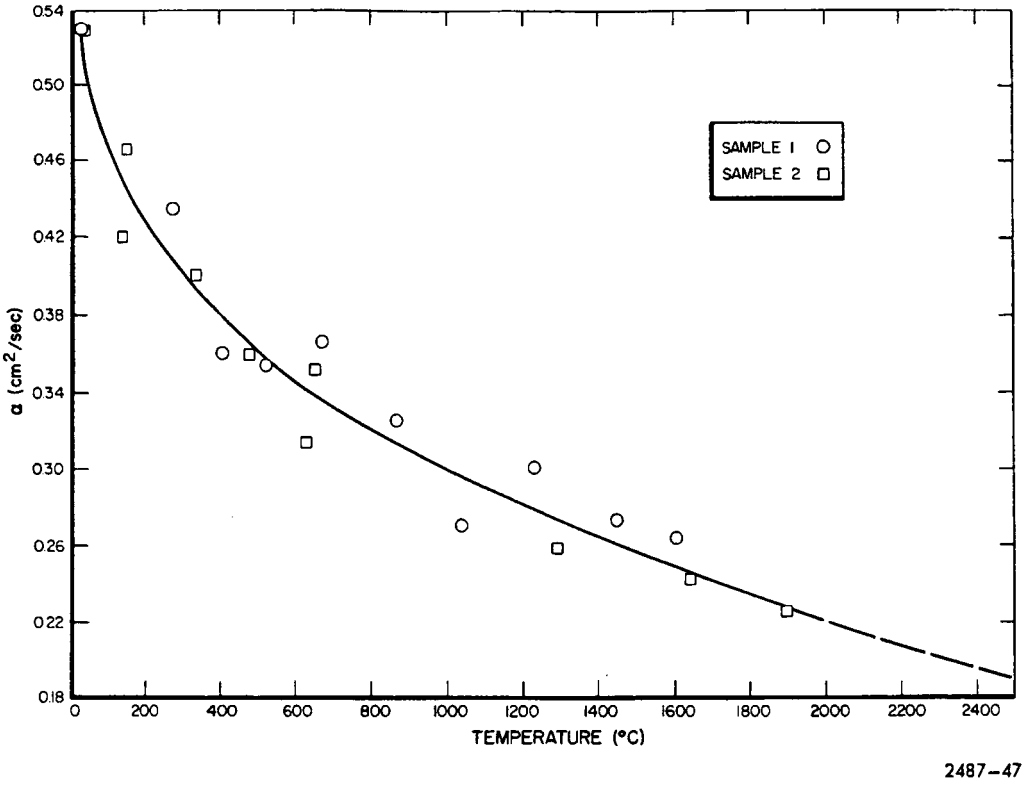

Figure 12. Thermal Diffusivity of 90 W - 10 UO_2 Mixture

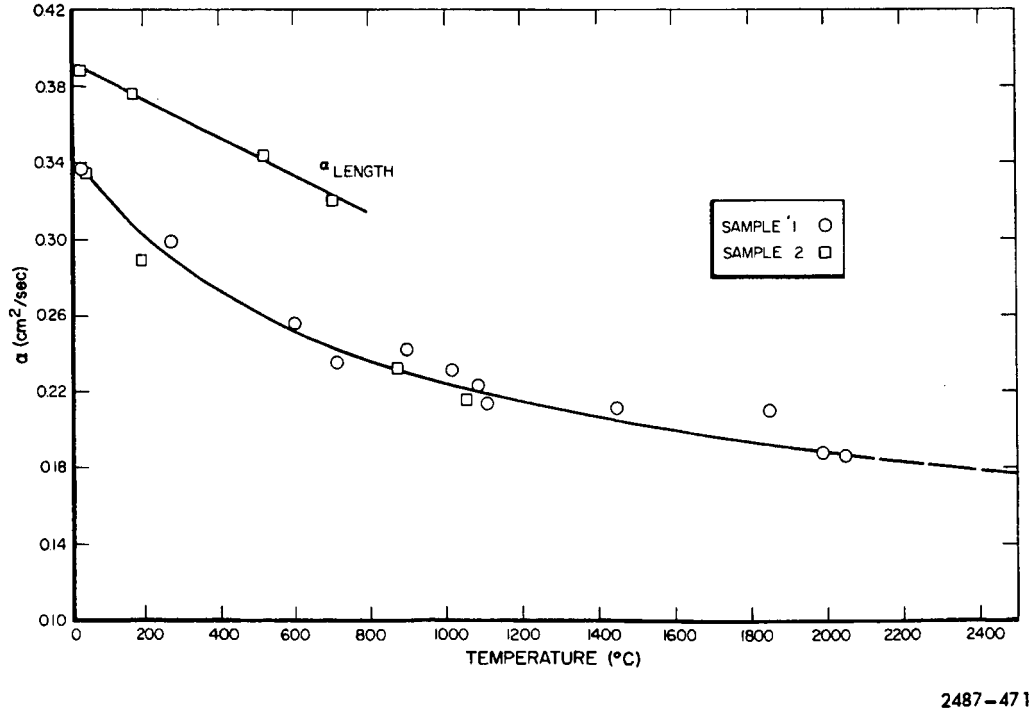

Figure 13. Thermal Diffusivity of 80 W - 20 UO_2 Mixture

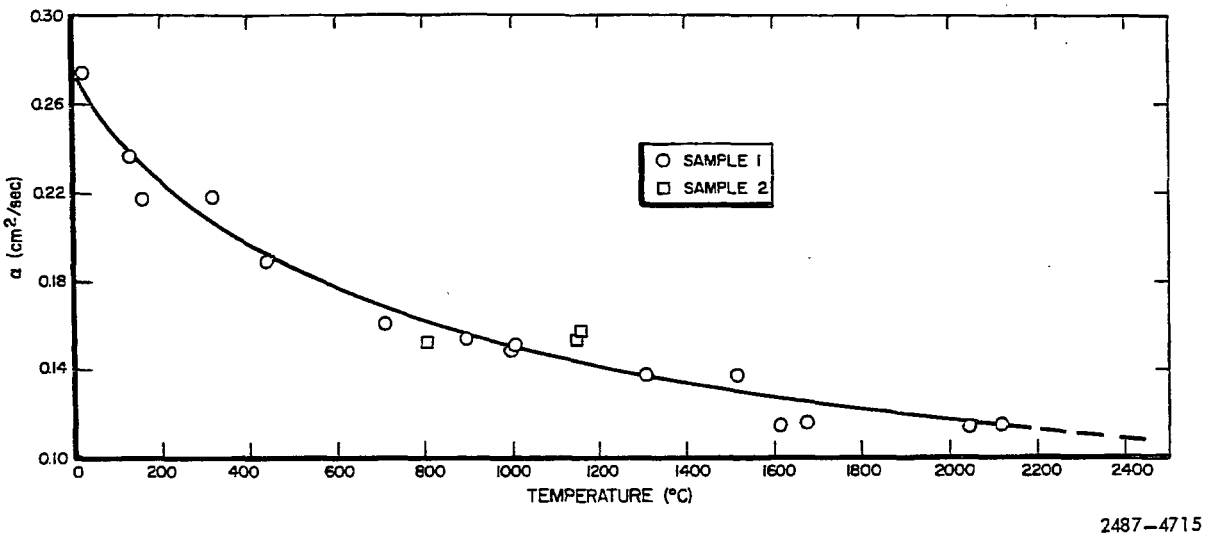

Figure 14. Thermal Diffusivity of 70 W - 30 UO_2 Mixture

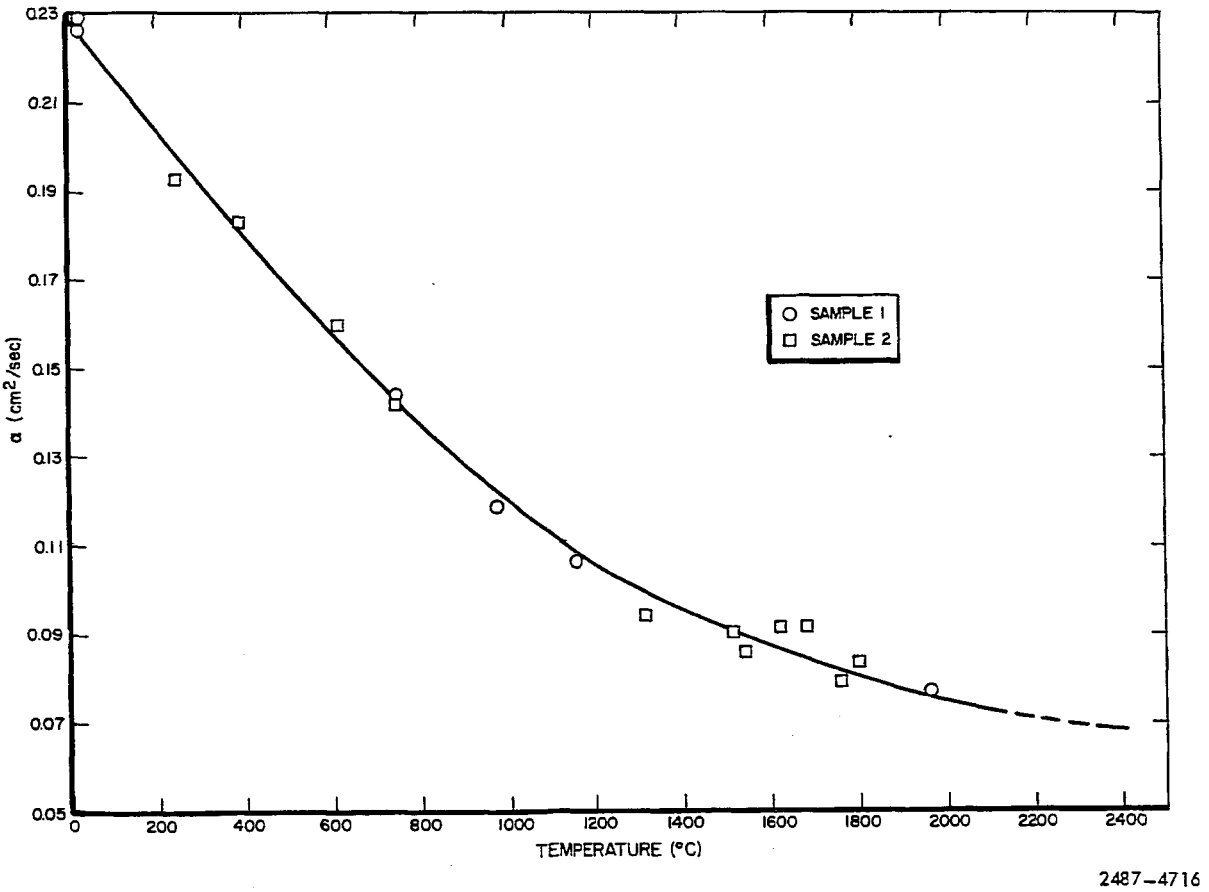

Figure 15. Thermal Diffusivity of 60 W - 40 UO_2 Mixture

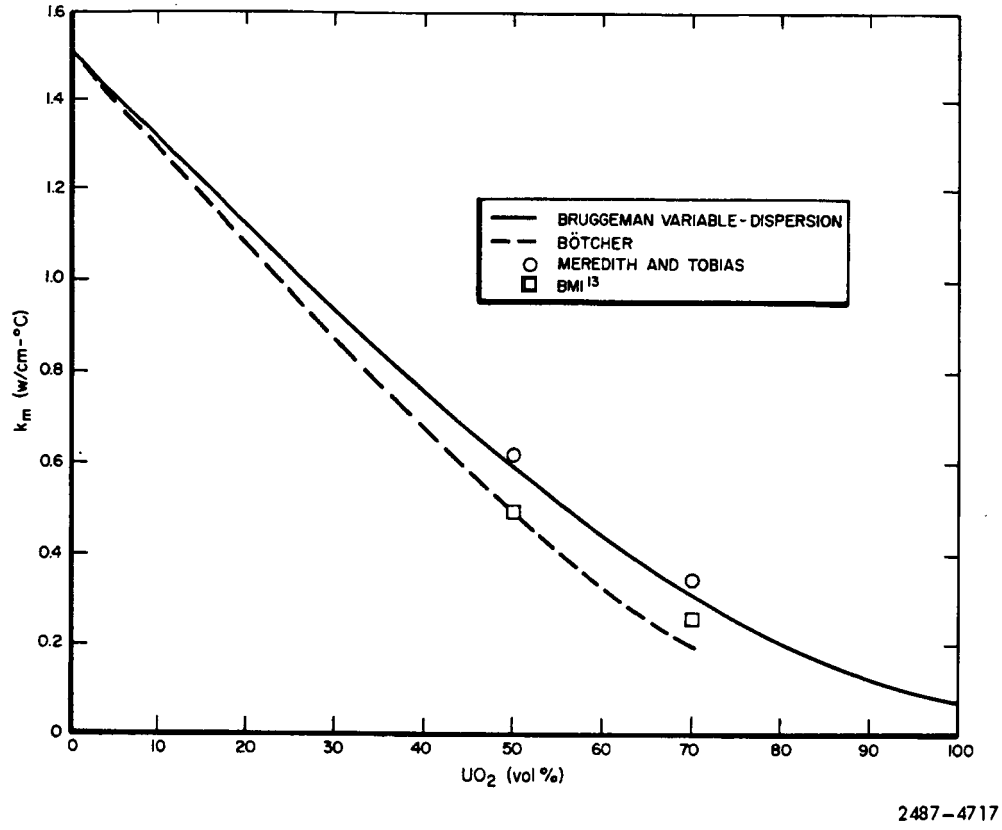

Figure 16. Thermal Conductivity of W-UO_2 Mixtures at 200°C

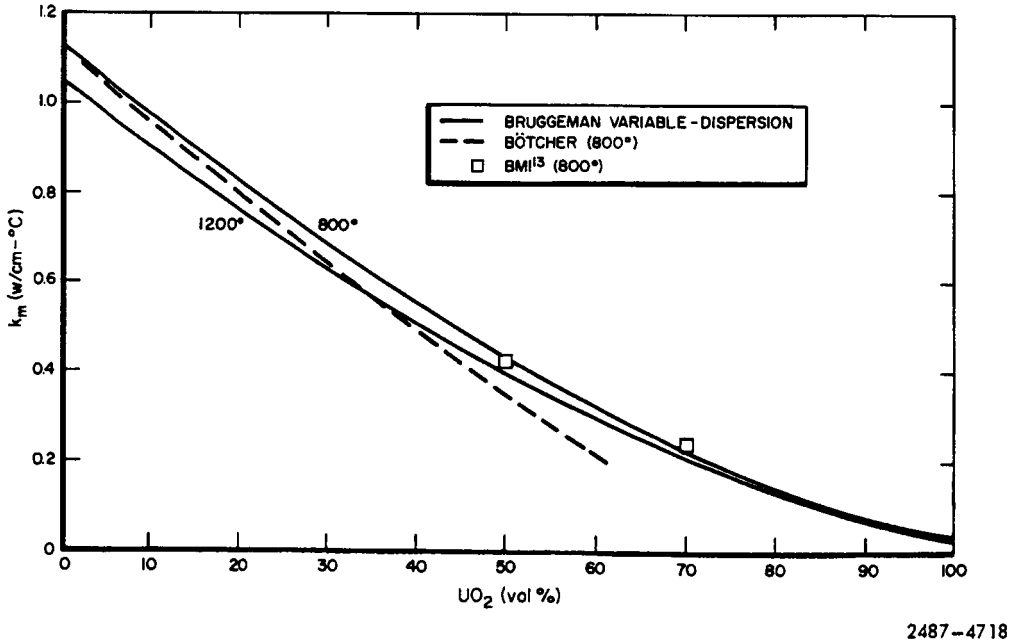

Figure 17. Thermal Conductivity of W-UO_2 Mixtures at 800 and 1200°C

VI. THERMAL CONDUCTIVITY

A. VALUES OBTAINED FROM MIXTURE CALCULATIONS

Numerous equations have been derived for the calculation of the thermal conductivities of mixtures, based upon the conductivities of the components. These equations have been summarized by Powers,[15] who classified the equations according to the basic assumptions concerning the nature of the mixture. Three equations, the Bruggeman variable-dispersion, the Bötcher, and the Meredith and Tobias, were investigated, since the assumptions made in their derivations are believed to be approximately true in the case of the W-UO_2 dispersions.

The Bruggeman variable-dispersion equation, which assumes that spherical particles are imbedded in a continuous phase, is given by

$$1-P_1 = \frac{K_1 - K_m}{K_1 - K_2}\left(\frac{K_2}{K_m}\right)^{1/3} \qquad \ldots(12)$$

where:

P_1 = volume fraction of the discontinuous phase

K_1 = conductivity of the discontinuous phase

K_2 = conductivity of the continuous phase

K_m = conductivity of the mixture.

For any given temperature, K_1 and K_2 are constant. Consequently, it is possible to plot K_m as a function of P_1, in order to determine the conductivity of any composition. Figure 16 is such a plot for W-UO_2 at 200°C. Experimental values, obtained by BMI on 50-50 and 30-70 vol% W-UO_2 mixtures,[16] are also shown in the figure. The calculated values are approximately 20% above the experimental results for both compositions. A similar plot for 800 and 1200°C is shown in Figure 17. From this figure, it can be seen that the experimental results are only a few percent different from the calculated values at 800°C. No experimental values were determined by BMI above 1000°C.[16]

Bötcher[15] devised an equation, based on the assumption that each particle is surrounded by a medium of K_m, and not necessarily surrounded completely by the opposite phase. It is:

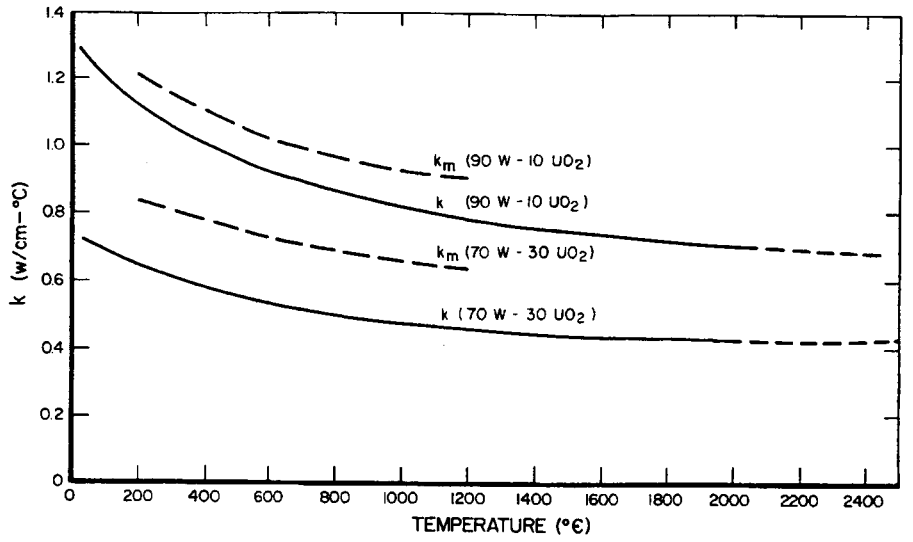

Figure 18. Thermal Conductivity of 90 W - 10 UO_2 and 70 W - 30 UO_2 Mixtures

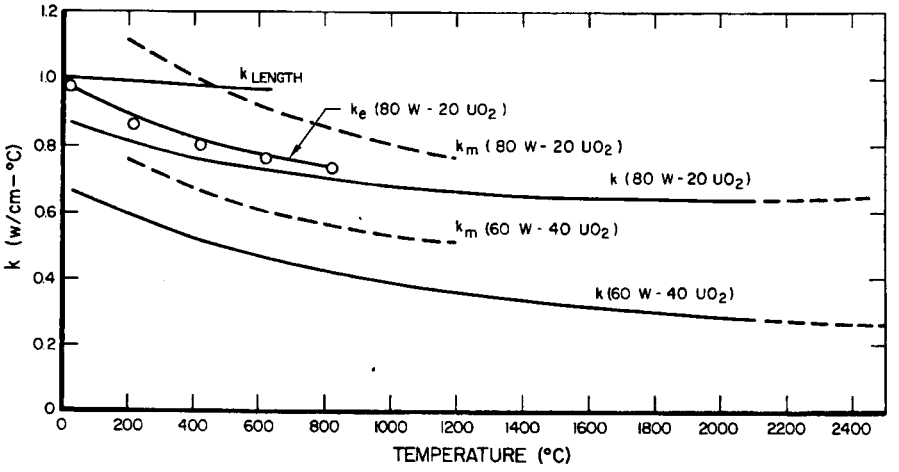

Figure 19. Thermal Conductivity of 80 W - 20 UO_2 and 60 W - 40 UO_2 Mixtures

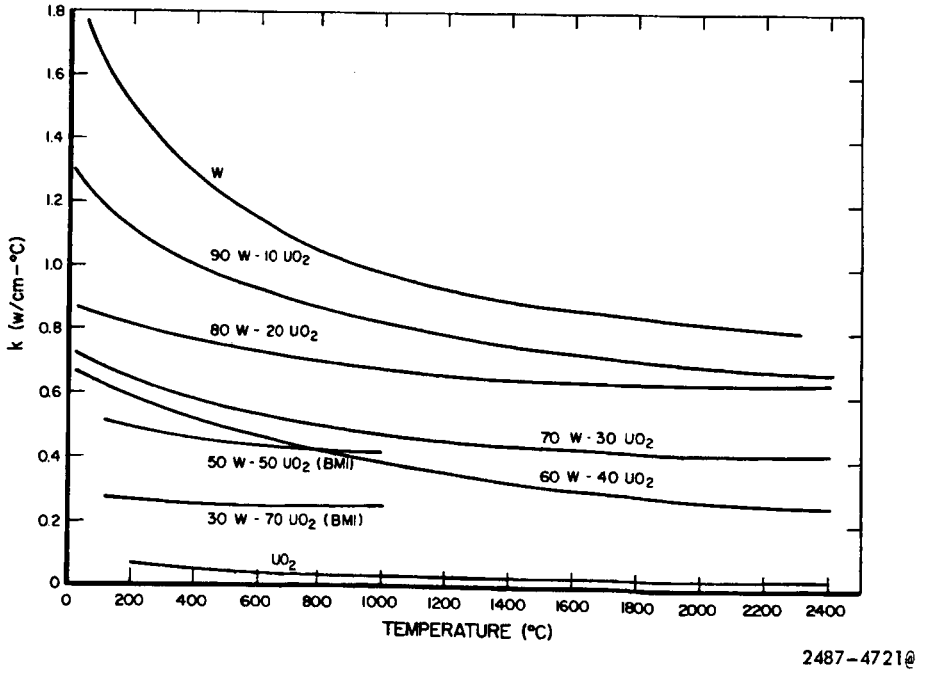

Figure 20. Thermal Conductivity of W-UO_2 Composites

$$\frac{K_m - K_1}{3K_m} = P_2 \frac{K_2 - K_1}{K_2 + 2K_m} \quad \ldots(13)$$

The results for W-UO_2 at 200°C are given in Figure 16, and the results at 800°C are included in Figure 17. It should be noted that the agreement between the experimental results and the calculated values is better at 200°C for the Bötcher equation, and better at 800°C for the Bruggeman variable-dispersion equation.

Recently, Meredith and Tobias,[15] using the Maxwell equation, derived a dispersion equation for variable concentrations, based on the assumption of only two particle sizes, rather than a large number of particle sizes, as assumed in the Bruggeman variable-dispersion equation. Their equation is:

$$K_m = K_2 \left[\frac{4K_2 + 2K_1 - 2P_1(K_2 - K_1)}{4K_2 + 2K_1 + P_2(K_2 - K_1)}\right] \left[\frac{4K_2 + 2K_1 - P_2(4K_2 - K_1)}{4K_2 + 2K_1 - P_2(K_2 + 2K_1)}\right] \quad \ldots(14)$$

As shown in Figure 16, the results of this equation are very close to that of the Bruggeman variable-dispersion equation.

The experimental results for the present samples are compared to the values calculated, using the Bruggeman variable-dispersion equation in the following sections.

B. VALUES OBTAINED FROM THERMAL DIFFUSIVITY

Equation 1 was used to compute the thermal conductivities of the various mixtures. These calculations are summarized in Appendix V.

The results for the 90-10 and 70-30 mixtures are plotted in Figure 18, and the results for the 80-20 and 60-40 mixtures are plotted in Figure 19. The conductivities of each of the mixtures decreases with increasing temperature; and, as noted in Section V, the conductivity is anisotropic.

The calculated values for k_m are also plotted in Figure 18 and 19. From these figures, it can be seen that k_m is greater than the experimentally observed k. This is due, at least in part, to the anisotropic effect, and is in semiquantitative agreement with predictions based on Power's report.[15]

The experimental thermal conductivity results, for the various composites and for pure W and UO_2, are summarized in Figure 20.

C. VALUES OBTAINED FROM ELECTRICAL RESISTIVITY

Contemporary theory states that the heat conduction in electrically conducting materials is the sum of the electronic conduction (k_e) and phonon (lattice) conduction (k_p), i.e.,

$$k_t = k_e + k_p \quad , \qquad \ldots(15)$$

where k_t is the total heat conductivity. The heat conduction due to electrons is given by the Wiedemann-Franz relation

$$k_e = \frac{LT}{\rho} \qquad \ldots(16)$$

where:

L = a constant, theoretically equal to 2.45×10^{-8} w-Ω/°K^2

T = the absolute temperature (°K)

ρ = the electrical resistivity, (Ω-cm)

Although the phonon conduction should follow a 1/T law, there is ample evidence that it may not do this.[17] In any event, the total conductivity must be equal to or greater than the electronic conductivity alone.

The electrical resistivity of the 80-20 material was measured by the dc potentiometric drop method, in which the voltage drop caused by the passage of a dc current through the sample is compared to the voltage drop across a standard resistor. The current is then reversed and the process repeated, in order to eliminate the effects of stray emfs.

The results, along with literature values for tungsten, are given in Figure 21. These values were used to calculate the thermal conductivity contributon due to electrons, and the results are plotted in Figure 19. Since the electrical resistivity was measured in the length direction, k_e should be compared to the k obtained for the length direction. When this is done, one notes that k_e is less

than k, as it should be, and that about 80% of the heat is transported by electrons at 400°C. This is in good agreement with the results from BMI.[16]

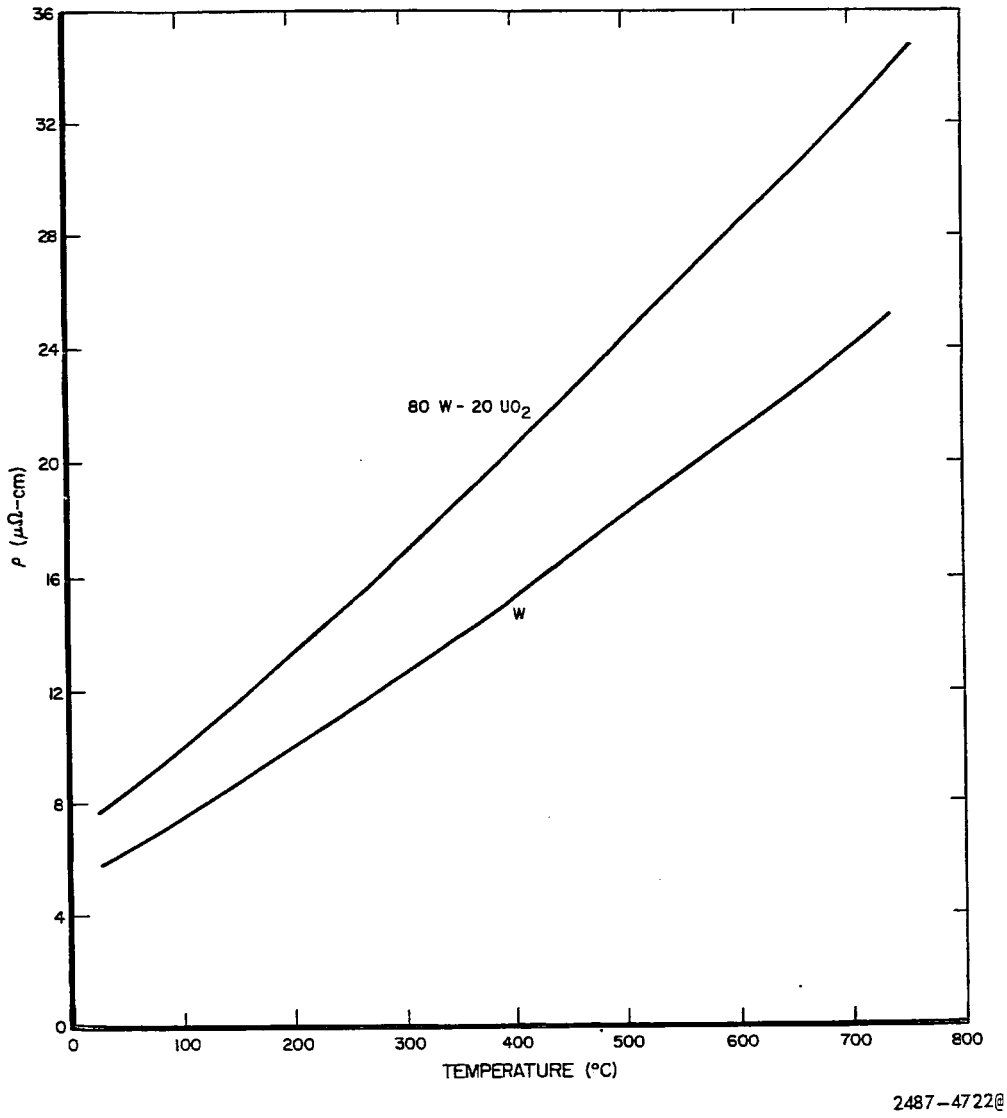

Figure 21. Electrical Resistivity of 80 W - 20 UO_2 Mixture

REFERENCES

1. F. E. Rom, P. G. Johnson, and R. E. Hyland, "Water-Moderated Nuclear Rockets," NASA TM-X482 (1961)

2. R. J. Buzzard and F. L. Gill, "High Temperature Mechanical Properties of a Tungsten-Uranium Dioxide Composite," NASA TM (E-2453) (1964)

3. N. T. Saunders, G. K. Watson, and R. J. Buzzard, "Investigation of Tungsten and Uranium Dioxide," Proceedings of Nuclear Propulsion Conference, August 15-19, 1962, Naval Postgraduate School, Monterey, California, TID-7553, Pt. II, Book 2

4. N. S. Rasor and J. D. McClelland, "Thermal Property Measurements at Very High Temperatures," Rev. Sci. Inst. 31, 595 (1960)

5. N. S. Rasor and J. D. McClelland, "Thermal Properties of Graphite, Molybdenum, and Tantalum to Their Destruction Temperatures," Int. J. Phys. Chem. of Solids 15, 17 (1960)

6. R. E. Taylor, "Thermal Conductivity and Expansion of Beryllia at High Temperatures," J. Am. Ceram. Soc. 45, 74 (1962)

7. C. J. Enberg and E. H. Zehms, "Thermal Expansion of Al_2O_3, BeO, MgO, B_4C, SiC, and TiC above 1000° C," J. Am. Ceram. Soc. 42, 300 (1959)

8. F. A. Mauer and L. H. Bolz, "Measurement of Thermal Expansion of Cermet Components of High Temperature X-ray Diffraction," WADC-TR-55-473 (December 1955)

9. J. Belle, Uranium Dioxide: Properties and Nuclear Applications, Naval Reactor, Division of Reactor Development, United States Atomic Energy Commission (1961)

10. V. A. Kirillin, A. E. Sheindlin, and V. Y. Chekhovskoy, "Enthalpy and Heat Capacity of Some Solid Materials at Extremely High Temperatures," Revised Supplement to Advance Papers, International Symposium on High Temperature Technology (September 8-11, 1963) Stanford Research Institute pp 110-133. Proceedings to be published by the International Union for Pure and Applied Chemistry.

11. H. L. Schick et al., "Thermodynamics of Certain Refractory Compounds," Part II, Fourth Quarterly Progress Report, RAD-SR-63-105 (June 1963)

12. W. J. Parker, R. J. Jenkins, C.P. Butler, and G. S. Abbott, "Flash Method of Determining Thermal Diffusivity, Heat Capacity, and Thermal Conductivity," J. App. Phys. 32, 1679 (1961)

13. R. E. Taylor and M. M. Nakata, "Thermal Properties of Refractory Materials," WADD-TR-60-581 Pt IV (November 1963)

REFERENCES

14. J. Cape and G. W. Lehman, "Temperature and Finite Pulse-Time Effects in the Flash Method for Measuring Thermal Diffusivity," J. Appl. Phys. 34, pp 1909-1913 (July 1963)

15. A. E. Powers, "Conductivity in Aggregates," KAPL-2145 (1961)

16. R. W. Dayton and R. F. Dickerson, "Progress Relating to Civilian Applications During February 1963," BMI-1619 (March 1963)

17. R. E. Taylor and J. Morreale, "Thermal Conductivity of Titanium Carbide, Zirconium Carbide, and Titanium Nitride at High Temperatures," J. Am. Ceram. Soc. 47, pp 69-73 (February 1964)

APPENDIX I
SAMPLE DENSITIES

	Sample Composition			
	90 W - 10 UO_2	80 W - 20 UO_2	70 W - 30 UO_2	60 W - 40 UO_2
Mass in air (g)	2.1494	1.1880	0.1979	1.3529
Mass in water (g)	2.0296	1.1192	0.1863	1.2692
Temperature of water (°C)	22.1	22.1	21.9	21.9
Volume of sample (cc)	0.1204	0.0692	0.0116	0.0841
Density of sample (g/cc)	17.85	17.17	17.06	16.09

APPENDIX II

THERMAL EXPANSION OF W-UO_2 MIXTURES

Sample	°C	°F	%E	Sample	°C	°F	%E	Sample	°C	°F	%E
90 W - 10 UO_2	276	529	0.13	80 W - 20 UO_2 (Edge)	2073	3763	1.24	60 W - 40 UO_2 (Continued)	1143	2089	0.75
	530	986	0.26		2250	4082	1.45		1145	2093	0.80
	534	993	0.26		2391	4336	1.47		1158	2116	0.84
	784	1443	0.39		2397	4347	1.43		1206	2203	0.75
	814	1497	0.41						1456	2653	0.86
	1030	1886	0.56	70 W - 30 UO_2	220	428	0.11		1488	2710	1.03
	1065	1949	0.53		508	946	0.26		1500	2732	1.05
	1091	1996	0.59		513	955	0.25		1530	2786	1.00
	1360	2480	0.69		771	1420	0.40		1578	2872	1.11
	1411	2572	0.77		810	1490	0.43		1622	2952	1.10
	1753	3187	0.93		987	1809	0.54		1681	3058	1.03
	2224	4035	1.23		1256	2293	0.71		1691	3076	1.20
	2495	4523	1.40		1299	2370	0.74		1817	3303	1.32
	2651	4804	1.54		1523	2773	0.84		1844	3351	1.33
					1694	3081	0.98		1873	3403	1.30
80 W - 20 UO_2	1026	1879	0.56		1853	3367	1.08		1964	3567	1.37
	1358	2476	0.70		1989	3612	1.14		2077	3771	1.39
	1404	2559	0.82		2238	4060	1.39		2090	3794	1.33
	1626	2959	0.87						2113	3835	1.59
	1719	3126	1.02						2196	3985	1.44
	1926	3499	1.04						2243	4069	1.58
	2088	3790	1.30	60 W - 40 UO_2	795	1463	0.51		2287	4149	1.57
	2201	3994	1.22		925	1697	0.63		2301	4174	1.77
	2395	4343	1.39		1063	1945	0.68		2343	4249	1.69
	2404	4359	1.50		1080	1976	0.57		2539	4602	1.87
	2494	4521	1.60		1100	2012	0.72		2552	4626	2.04
	2664	4827	1.74		1133	2071	0.80		2633	4771	1.99

APPENDIX III
FINITE PULSE TIME EFFECT

Using the notation of Cape and Lehman's paper,[14] the heat flow can be expressed as

$$(k/q_o)\delta(a,r,t) = D_o(r,y_r) \sum_{m=o}^{\infty} C_m X_m \int_o^t dt' W(t') \exp\left[\omega_{om}(t - t')/t_c\right] \quad \ldots(17)$$

For a square wave input,

$$W(t') = \tau \ , \quad t \leq \tau$$

$$= o \ , \quad t > \tau$$

For a radiationless case,

$$C_m X_m = 2\left(\frac{\alpha}{a}\right)(-1)^m \ , \qquad m = 1,2,3\ldots$$

$$C_o X_o = \frac{\alpha}{a}$$

$$\omega_{oo} = o$$

$$\omega_{om} = -m^2 \ , \qquad m = 1,2,3\ldots \ .$$

for $t \leq \tau$,

$$(k/q_o)\delta(a,r,t) = D_o(r,y_r)\frac{\alpha}{a}\left\{\int_o^t dt'\frac{1}{\tau} + \frac{2}{\tau}\sum_{m=1}^{\infty}\int_o^t dt' \exp\left[-m^2(t - t')/t_c\right]\right\}$$

$$= D_o(r,y_r)\frac{\alpha}{a}\left\{\frac{t}{\tau} + 2\frac{t_c}{\tau}\sum_{m=1}^{\infty}\frac{(-1)^m}{m^2}\left[1 - \exp\left(-m^2 t/t_c\right)\right]\right\} \ . \quad \ldots(18)$$

for $t > \tau$,

$$(k/q_o)\delta(a,r,t) = D_o(r,y_r)\frac{\alpha}{a}\left\{\int_o^{\tau} dt'\frac{1}{\tau} + \frac{2}{\tau}\sum_{m=1}^{\infty}(-1)^m \int_o^{\tau} dt' \exp\left[-m^2(t - t')/t_c\right]\right\}$$

$$= D_o(r,y_r)\frac{\alpha}{a}\left\{1 + \frac{2t_c}{\tau}\sum_{m=1}^{\infty}\frac{(-1)^m}{m^2}\exp(-m^2 t/t_c)[\exp(m^2\tau/t_c)-1]\right\} \quad \ldots(19)$$

But, for $t = \infty$,

$$k/q_o\delta(a,r,\infty) = D_o(r,y_r)\frac{\alpha}{a} \quad . \qquad \ldots(20)$$

Therefore,

$$\frac{\delta(a,r,t)}{\delta(a,r,\infty)} = \frac{t}{\tau} + 2\frac{t_c}{\tau}\sum_{m=1}^{\infty}\frac{(-1)^m}{m^2}[1 - \exp(-m^2 t/t_c)] \quad , \quad t \le \tau \qquad \ldots(21)$$

$$\frac{\delta(a,r,t)}{\delta(a,r,\infty)} = 1 + 2\frac{t_c}{\tau}\sum_{m=1}^{\infty}\frac{(-1)^m}{m^2}\exp(-m^2 t/t_c)[\exp(m^2\tau/t_c)-1] \quad t \ge \tau \qquad \ldots(22)$$

APPENDIX IV

THERMAL DIFFUSIVITIES OF W-UO_2 MIXTURES

Sample	Temperature (°C)	Diffusivity (cm^2/sec)	Sample	Temperature (°C)	Diffusivity (cm^2/sec)
90 W - 10 UO_2	25	0.530	70 W - 30 UO_2	708	0.160
1	272	0.434	1	895	0.154
	521	0.354		997	0.148
	677	0.369		1004	0.150
	402	0.361		1305	0.137
	863	0.326		1511	0.137
	1039	0.270		1608	0.115
	1230	0.301		1671	0.116
	1459	0.274			
	1602	0.265	2	392	0.168
				804	0.153
2	477	0.360		1157	0.157
	628	0.315		1147	0.153
	650	0.353		2050	0.155
	336	0.404		2115	0.115
	152	0.465		25	0.275
	30	0.530		128	0.237
	136	0.420		152	0.217
	1298	0.259		311	0.219
	1644	0.242		437	0.189
	1900	0.225			
			60 W - 40 UO_2	25	0.229
80 W - 20 UO_2	25	0.338		744	0.144
1	270	0.298		1152	0.107
	595	0.255	2	970	0.119
	709	0.235			
	900	0.243	2	25	0.227
	1022	0.231		239	0.193
	1102	0.214		393	0.182
	1088	0.223		615	0.160
	1450	0.212		745	0.142
	1850	0.220		1315	0.0946
	1990	0.187		1541	0.0868
	2050	0.185		1615	0.0925
				1685	0.0925
2	25	0.338		1753	0.0791
	176	0.289		1510	0.0909
	868	0.233		1790	0.0843
	1052	0.214		1958	0.0778
80 W - 20 UO_2	25	0.389			
1	170	0.377			
(Length Direction)	513	0.344			
	700	0.320			

APPENDIX V

THERMAL CONDUCTIVITIES OF W-UO_2 COMPOSITES

Temperature (°K)	c_p (cal/g-°C)	α (cm^2/sec)	d (g/cc)	k (w/cm-°C)
	90 W - 10 UO_2 Mixture			
300	0.0330	0.530	17.85	1.307
500	0.0340	0.423	17.85	1.065
700	0.0350	0.376	17.85	0.983
900	0.0358	0.343	17.85	0.917
1100	0.0367	0.318	17.85	0.872
1300	0.0375	0.297	17.85	0.832
1500	0.0385	0.279	17.85	0.803
1700	0.0393	0.263	17.85	0.772
1900	0.0401	0.248	17.85	0.743
2100	0.0409	0.234	17.85	0.715
2300	0.0420	0.220	17.85	0.690
2500	0.0437	0.208	17.85	0.679
2700	0.0463	0.196	17.85	0.678
	80 W - 20 UO_2 Mixture			
300	0.0360	0.337	17.17	0.872
500	0.0385	0.288	17.17	0.797
700	0.0395	0.270	17.17	0.766
900	0.0406	0.250	17.17	0.730
1100	0.0417	0.235	17.17	0.704
1300	0.0426	0.222	17.17	0.680
1500	0.0435	0.213	17.17	0.666
1700	0.0445	0.206	17.17	0.659
1900	0.0452	0.198	17.17	0.643
2100	0.0461	0.193	17.17	0.639
2300	0.0472	0.188	17.17	0.638
2500	0.0490	0.183	17.17	0.644
2700	0.0515	0.179	17.17	0.662
	80 W - 20 UO_2 in the Width Direction			
300	0.0360	0.388	17.17	1.00
500	0.0385	0.370	17.17	1.02
700	0.0395	0.350	17.17	0.994
900	0.0406	0.330	17.17	0.963

Temperature (°K)	c_p (cal/g-°C)	α (cm^2/sec)	d (g/cc)	k (w/cm-°C)
	70 W - 30 UO_2 Mixture			
300	0.0377	0.268	17.06	0.721
500	0.0406	0.220	17.06	0.638
700	0.0422	0.193	17 06	0.582
900	0.0435	0.175	17.06	0.544
1100	0.0447	0.160	17.06	0.511
1300	0.0456	0.148	17.06	0.482
1500	0.0465	0.140	17.06	0.465
1700	0.0474	0.132	17.06	0.447
1900	0.0482	0.126	17.06	0.434
2100	0.0492	0.121	17.06	0.425
2300	0.0503	0.116	17.06	0.417
2500	0.0520	0.112	17.06	0.419
2700	0.0545	0.108	17.06	0.420
	60 W - 40 UO_2 Mixture			
300	0.0395	0.226	16.09	0.601
500	0.0431	0.202	16.09	0.592
700	0.0452	0.178	16.09	0.542
900	0.0467	0.155	16.09	0.487
1100	0.0478	0.135	16.09	0.435
1300	0.0488	0.118	16.09	0.388
1500	0.0497	0.104	16.09	0.348
1700	0.0508	0.0940	16.09	0.322
1900	0.0515	0.0870	16.09	0.302
2100	0.0525	0.0800	16.09	0.283
2300	0.0538	0.0742	16.09	0.269
2500	0.0555	0.0705	16.09	0.264
2700	0.0578	0.0680	16.09	0.265

REPORT DISTRIBUTION LIST
FOR
CONTRACT NAS3-4280

Space Nuclear Propulsion Office
Washington, D. C.
Attn: J. Morrisey

NASA Headquarters
Washington, D. C.
Attn: G. Deutsch

AEC Headquarters
Division of Reactor Development
Washington, D. C.
Attn: S. Christopher

Argonne National Laboratory (2)
Argonne, Illinois
Attn: J. Schumar
Attn: R. Noland

Hanford Laboratories
Richland, Washington
Attn: F. Albaugh

Oak Ridge Gaseous Diffusion Plant
Oak Ridge, Tennessee
Attn: P. Huber

General Electric - NMPO
Evandale, Ohio
Attn: J. McGurty

Battelle Memorial Institute
Columbus, Ohio
Attn: E. Hodge

Nuclear Materials & Equipment Corp.
Apollo, Pennsylvania
Attn: B. Vondra

Sylvania Electric Products
Chemical & Metallurgical Division
Towanda, Pennsylvania
Attn: M. MacInnis

Westinghouse Electric Corporation
Astronuclear Laboratory
Pittsburgh, Pennsylvania
Attn: D. Thomas

United Nuclear Corporation
New Haven, Connecticut
Attn: E. Gordon

Union Carbide Corporation
Nuclear Products Department
Lawrenceburg, Tennessee
Attn: W. Eatherly

General Atomics Division
General Dynamics Corporation
San Diego, California
Attn: A. Weinburg

Atomics International Division
North American Aviation, Inc.
Canoga Park, California
Attn: S. Carniglia

Minnesota Mining & Manufacturing Company
Nuclear Products Department
St. Paul, Minnesota
Attn: J. Ryan

Martin Marietta Corporation
Nuclear Division
Baltimore, Maryland
Attn: C. Eicheldinger

NASA Lewis Research Center (20)
21000 Brookpark Road
Cleveland, Ohio 44135
Attn: R. Buzzard (10)
N. Saunders
S. Kaufman (3)
A. Lietzke (2)
T. Moss
J. Creagh
H. Smreker
Nuclear Rocket Technology Office

NASA Lewis Research Center (1)
21000 Brookpark Road
Cleveland, Ohio 44135
Attn: John J. Fackler, Contracting Officer

NASA Lewis Research Center (1)
21000 Brookpark Road
Cleveland, Ohio 44135
Attn: Norman T. Musial

NASA Scientific & Technical Information Facility
(1 + reproducible)
Box 5700
Bethesda, Maryland
Attn: NASA Representative

NASA Lewis Research Center (2)
21000 Brookpark Road
Cleveland, Ohio 44135
Attn: Library

NASA Lewis Research Center (1)
21000 Brookpark Road
Cleveland, Ohio 44135
Attn: Reports Control Office

U. S. Atomic Energy Commission (1)
Technical Reports Library
Washington, D. C.

U. S. Atomic Energy Commission (1)
Technical Information Service Extension
P. O. Box 62
Oak Ridge, Tennessee

NASA Lewis Research Center (1)
21000 Brookpark Road
Cleveland, Ohio 44135
Attn: Office of Reliability and Quality Assurance

NASA Ames Research Center (1)
Moffett Field, California 94035
Attn: Library

NASA Flight Research Center (1)
P. O. Box 273
Edwards, California 93523
Attn: Library

NASA Goddard Space Flight Center (1)
Greenbelt, Maryland 20771
Attn: Library

Jet Propulsion Laboratory (1)
4800 Oak Grove Drive
Pasadena, California 91103
Attn: Library

NASA Langley Research Center (1)
Langley Station
Hampton, Virginia 23365
Attn: Library

NASA Manned Spacecraft Center (1)
Houston, Texas 77001
Attn: Library

NASA Marshall Space Flight Center (1)
Huntsville, Alabama 35812
Attn: Library

NASA Western Operations (1)
150 Pico Boulevard
Santa Monica, California 90406
Attn: Library